Available online at www.sciencedirect.com

ScienceDirect

Ceramics International 40 (2014) 5289–5298

CERAMICS INTERNATIONAL

www.elsevier.com/locate/ceramint

Sintering, microstrusture and hardness of different alumina–zirconia composites

Heidy L. Calambás Pulgarin, María P. Albano*

Centro de Tecnología de Recursos Minerales y Cerámica (CETMIC), C.C. 49 (B1897ZCA) M. B. Gonnet, Provincia de Buenos Aires, Argentina

Received 2 September 2013; received in revised form 7 October 2013; accepted 20 October 2013
Available online 31 October 2013

Abstract

Two commercial 3 mol% yttria-partially stabilized zirconia powders, 0.3 wt% Al_2O_3-doped (Al-doped Y-PSZ) and without Al_2O_3 (Y-PSZ), were used to produce alumina (Al_2O_3)-zirconia (ZrO_2) slip cast composites. The influence of the substitution of Al_2O_3 either by different Al-doped Y-PSZ contents or 50 vol% Y-PSZ on the sintering kinetic at the intermediate stage was investigated. In addition, the microstructure of Al_2O_3 and the different composites at temperatures in the range of 1100–1600 °C was studied and related to the sample hardness. An increase in the sintering rate was observed when Al-doped Y-PSZ increased from 22 to 50 vol% or when 50 vol% Y-PSZ was substituted by 50 vol% Al-doped Y-PSZ. 50 vol% ZrO_2 was the most effective concentration to reduce the rate of Al_2O_3 grain growth in the final sintering stage; the Al_2O_3 grain growth began at lower temperatures and became greater with decreasing the Al-doped Y-PSZ content. On the contrary, the ZrO_2 grain growth slightly increased with increasing the Al-doped Y-PSZ concentration. However, for 50 vol% Al-doped Y-PSZ a smaller ZrO_2 grain size distribution compared with 50 vol% Y-PSZ could be achieved. As the average Al_2O_3 grain size of the sintered samples became greater than about 1 μm a markedly decrease in the hardness was found; this occurred at temperatures higher than 1400 °C and 1500 °C for Al_2O_3 and the composite with 10.5 vol% Al-doped Y-PSZ, respectively.

Keywords: Al_2O_3–ZrO_2; Sintering behavior; Microstructure; Hardness

1. Introduction

Recently, zirconia-toughened-alumina ceramics have received considerable attention due to their attractive properties, including high-temperature mechanical strength, good thermal shock resistance, wear and oxidation resistance, low thermal conductivity, and the close match between their thermal expansion coefficients and those of metals [1,2]. These properties make zirconia–alumina ceramics suitable for a variety of high demanding applications including dental screws, cutting blades, electrosurgical insulators, valve seals, body armor, pump components, oxygen sensors, dies, and prosthesis components such as hip joints [3,4]. The zirconia grains embedded in an alumina matrix enhance the flexural strength, fracture toughness, and fatigue resistance [5]. The toughening mechanisms identified in zirconia-reinforced alumina ceramics is attributed to the stress induced phase transformation of metastable tetragonal grains towards the monoclinic symmetry ahead of a propagating crack, leading to an increase in the work of fracture [5]. This phenomenon of transformation toughening relies on the volume expansion, 3–5%, and shear strain $\approx 7\%$ develops when tetragonal zirconia transforms to the monoclinic form [6]. Besides, microcracks extending in the stress field of a propagating crack can absorb the fracture energy, increasing the material toughness by the microcrack toughening mechanism [2]. However, studies on the application of these materials in humid environment at low temperature have shown that the tetragonal → monoclinic transformation can also be induced at the surface of ZrO_2 grains, leading to the so-called hydrothermal transformation or ageing behavior of zirconia, which produces a slow degradation of the composite mechanical properties [3]. Alumina has lower susceptibility to water and thus to stress assisted corrosion than zirconia, consequently the use of 0.3 wt% Al_2O_3-doped Y-PSZ to develop alumina–zirconia ceramics might be beneficial to minimize the ageing phenomenon of zirconia, increasing the stability of

*Corresponding author. Tel.: +54 221 484 0247; fax: +54 221 471 0075.
E-mail address: palbano@cetmic.unlp.edu.ar (M.P. Albano).

0272-8842/$ - see front matter © 2013 Elsevier Ltd and Techna Group S.r.l. All rights reserved.
http://dx.doi.org/10.1016/j.ceramint.2013.10.102

the composites under hydrothermal conditions. Stability and hardness are of prime interest in the orthopedic field; high hardness of the composites should lead a priori to higher wear resistance [6]. Therefore, alumina–zirconia composites with different Al-doped Y-PSZ contents were produced and their sintering kinetic, microstructure and hardness were investigated.

Two commercial 3 mol% yttria-partially stabilized zirconia powders, 0.3 wt% Al_2O_3-doped (Al-doped Y-PSZ) and without Al_2O_3 (Y-PSZ), were used to produce Al_2O_3–ZrO_2 slip cast composites. The different contents of Al-doped Y-PSZ powder and also the different physical and chemical characteristics of the two zirconia powders were believed to strongly affect the sintering kinetic and the microstructure development of the Al_2O_3–ZrO_2 composites. The sintering of Al_2O_3 and ZrO_2 powders has been investigated previously by many researchers, and several sintering-rate equations have been reported and used for the kinetic analysis at the intermediate sintering stage [7,8]. However, the effect of both the different Al-doped Y-PSZ contents and the substitution of 50 vol% Al-doped Y-PSZ by Y-PSZ, on the intermediate sintering stage of Al_2O_3–ZrO_2 composites have not been studied.

In this work, the influence of the substitution of Al_2O_3 either by different Al-doped Y-PSZ contents or 50 vol% Y-PSZ on the sintering kinetic at the intermediate stage was investigated. In addition, the microstructure of Al_2O_3 and the different composites at temperatures in the range of 1100–1600 °C was studied and related to the sample hardness.

2. Experimental procedure

2.1. Raw materials and powder processing

Alumina (A16 SG, Alcoa Chemicals, USA, d_{50}=0.40 μm), 3 mol% yttria- partially stabilized zirconia with 0.3 wt% Al_2O_3 (Saint-Gobain ZirPro, CY3Z-MA, Chine, d_{50}=0.23 μm) and without Al_2O_3 (Saint-Gobain ZirPro, CY3Z-NS, Chine, d_{50}=0.64 μm) powders were used in this study. The compositions used to prepare Al_2O_3–ZrO_2 composites are summarized in Table 1. The numbers 10.5, 22 and 50 in the sample codes indicate the volume percent of zirconia in the composite.

A commercial ammonium polyacrylate solution (NH_4PA) (Duramax D 3500, Rohm & Haas, Philadelphia PA) was used as deflocculant. 48 vol% aqueous Al_2O_3–ZrO_2 suspensions with the different compositions (Table 1) and the optimum NH_4PA concentration were prepared by suspending particles in deionized water via 40 min of ultrasound; the pH was manually adjusted to be maintained at 9 with ammonia (25%). Slips were cast in plaster molds into rectangular bars ($12 \times 10 \times 9$ mm^3); the consolidated bars were dried slowly in air for 24 h at room temperature and 24 h at 100 °C. The green samples were sintered in air at 1100–1600 °C for 2 h (heating rate 5 °C/min).

2.2. Characterization techniques

The specific surface area (S_g) and the particle size distribution of the powders were measured using a Micromeritics Accusorb and a Sedigraph (Micromeritics), respectively. The morphological features of the powders were examined by scanning electron microscopy (SEM) (JEOL, JSM-6360).

The density of the green compacts was determined by the Archimedes method using mercury displacement. The bulk density of the sintered samples was determined by water immersion (Standard Method ASTM C20). The sintered samples were polished with a series of diamond pastes down to 1/4 μm. The Vickers hardness (H_v) was carried out using a diamond indenter (Buehler hardness tester) at a load of 3 Kgf with an indentation period of 30 s. Ten H_v measurements were used to obtain an average value. The alumina and zirconia grain sizes were measured using SEM micrographs (JEOL, JSM-6360) of polished and thermally etched surfaces. The grain size values were the average of about a hundred measurements.

The isothermal shrinkage measurements were performed as follows: the temperature of the specimens was first increased at a constant rate of 10 °C/min to 800 °C, held at that temperature for 10 min, and subsequently increased rapidly at about 50 °C/min to the set temperature, which was in the range of 1150–1400 °C. The length shrinkage was measured as a function of time at the constant set temperature for 2 h. When the time reached 2 h, the specimens were cooled at a constant rate of 10 °C/min.

3. Results and discussion

3.1. Powder characterization

Fig. 1 shows the particle size distribution curves of the Al_2O_3, Y-PSZ and Al-doped Y-PSZ powders. The particle size distribution curves of Al_2O_3 and Al-doped Y-PSZ powders were similar. Alumina showed an unimodal distribution with

Table 1
Compositions used for the preparation of Al_2O_3–ZrO_2 composites.

Sample[a]	Al_2O_3 (vol%)	Al-doped Y-PSZ (vol%)	Y-PSZ (vol%)
10.5Al-doped Y-PSZ	89.5	10.5	–
22Al-doped Y-PSZ	78	22	–
50Al-doped Y-PSZ	50	50	–
50Y-PSZ	50	–	50

[a]The numbers 10.5, 22 and 50 in the sample codes indicate the volume percent of zirconia in the composite.

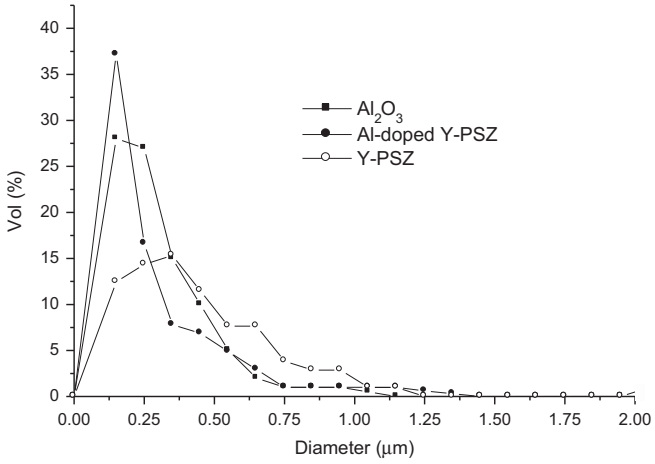

Fig. 1. Particle size distribution curves of different powders.

particle diameters >0.1 and <0.75 μm, the more frequent particle diameters were in the range of 0.15–0.3 μm. A slightly narrow particle size distribution was found for Al-doped Y-PSZ; thus a greater volume of finer particles (diameters between 0.10 and 0.20 μm) and a lesser volume of particles with diameters in the range of 0.20–0.55 μm were observed; the more frequent particle diameter was 0.15 μm. A bimodal distribution curve was found for Y-PSZ, the more frequent particle diameters (0.37 and 0.65 μm) were greater than those of Al_2O_3 and Al-doped Y-PSZ powders. A lesser volume of finer particles (<0.40 μm) and a greater volume of particles with diameters in the range of 0.40–1.05 μm were observed.

The specific surface areas (S_g) of Al_2O_3, Y-PSZ and Al-doped Y-PSZ powders were 8.74, 7.84 and 12.25 m^2/g, respectively. Fig. 2a–c shows SEM micrographs of Al_2O_3, Y-PSZ and Al-doped Y-PSZ, respectively. The shape of Al-doped Y-PSZ particles was different with respect to that of Al_2O_3 and Y-PSZ; Al_2O_3 and Y-PSZ particles showed smooth and sharp edges while Al-doped Y-PSZ presented round and rough ones; this last shape contributed to an increase in the S_g of Al-doped Y-PSZ powder. As we have mentioned Al-doped Y-PSZ powder contained 0.3 wt% Al_2O_3, phase equilibrium studies have shown that Al_2O_3 and ZrO_2 are compatible [9]; Al_2O_3 does not form solid solution with zirconia due to its low solubility, consequently Al_2O_3 is present in zirconia as a distinct phase and a mixture of ZrO_2 particles with fine Al_2O_3 particles is expected for Al-doped Y-PSZ. The finer particles and the particle shape of Al-doped Y-PSZ were responsible to its higher specific surface area with respect to that of Al_2O_3 and Y-PSZ.

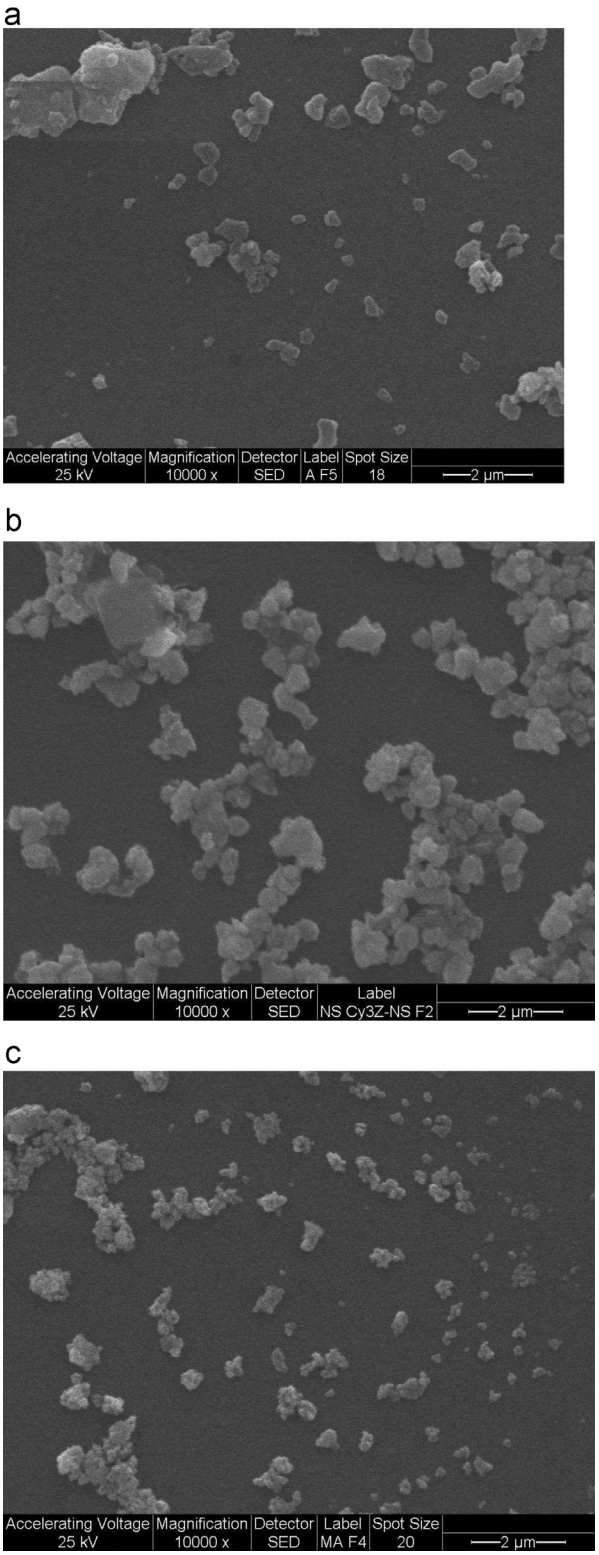

Fig. 2. SEM micrographs of different powders: (a) Al_2O_3, (b) Y-PSZ and (c) Al-doped Y-PSZ.

3.2. Densification and grain growth

Green density values of 63.2%, 62.5% and 60% of the theoretical density were measured for 10.5, 22 and 50Al-doped Y-PSZ, respectively. In a recent paper [10] we compared the green density of the different Al_2O_3–ZrO_2 composites and related them to the degree of slip dispersion; a less dense particle packing with increasing the slip viscosity was found. The substitution of Al_2O_3 by Al-doped Y-PSZ in the Al_2O_3–ZrO_2 mixtures increased the slip viscosity with NH_4PA resulting in a less dense packing of cast samples [10]. 50Y-PSZ slips exhibited a lower viscosity with respect to that of 50 Al-doped

Y-PSZ ones and resulted in a higher green density value of 65.3% of theoretical density [10].

Fig. 3 shows the change in the relative sintered density with sintering temperature of Al_2O_3 and the different composites. The respective derivatives of sintered density with respect to temperature are shown in Fig. 4. The densification rate of Al_2O_3 at the intermediate sintering stage was higher than that of the Al_2O_3–ZrO_2 composites. For 10.5 and 22Al-doped Y-PSZ the relationship between the relative density and the sintering temperature showed nearly the same behavior. When the Al-doped Y-PSZ concentration increased from 22 to 50 vol % the sintering began at lower temperatures and a higher relative density in the temperature range 1200–1400 °C could be found; thus, the densification rate increased.

The dρ/dT vs. T curves in Fig. 4 show a maximum, a higher peak temperature and a greater height of the peak were found for the Al_2O_3–Al-doped Y-PSZ composites relative to that of Al_2O_3. The addition of 10.5 and 22 vol% Al-doped Y-PSZ shifted the peak temperature of Al_2O_3 from 1300 to 1400 °C; whereas for 50Al-doped Y-PSZ a lesser displacement of the peak temperature to 1350 °C was found. Thus, 10.5 and 22Al-doped Y-PSZ required significantly higher temperatures for sintering than pure alumina; however, for 50Al-doped Y-PSZ an intermediate sintering temperature between that of Al_2O_3 and 22Al-doped Y-PSZ was necessary. This behavior was consistent with Wang et al. results [7] who reported the apparent retardation of the Al_2O_3 sintering rate in the presence of 5 vol% ZrO_2. The densification rate of 50Y-PSZ up to 1300 °C was lower than that of Al_2O_3 and Al-doped Y-PSZ; 50Al-doped Y-PSZ began to sinter at lower temperatures with respect to 50Y-PSZ and higher relative densities at 1250–1400 °C could be achieved (Figs. 3 and 4).

In order to investigate the accelerated sintering rate of Al_2O_3 and the enhanced sintering effect of 50Al-doped Y-PSZ with respect to the others composites, the isothermal shrinkage behavior of Al_2O_3 and Al_2O_3–ZrO_2 compacts was examined. Both values of the activation energy and the frequency-factor term in the applied sintering-rate equations were estimated from the isothermal shrinkage curves. The sintering-rate equation of isothermal shrinkage is given by [11]

$$\frac{\Delta L}{L_0} = \left(\frac{K\gamma\Omega D}{kTa^p}\right)^n t^n \quad (1)$$

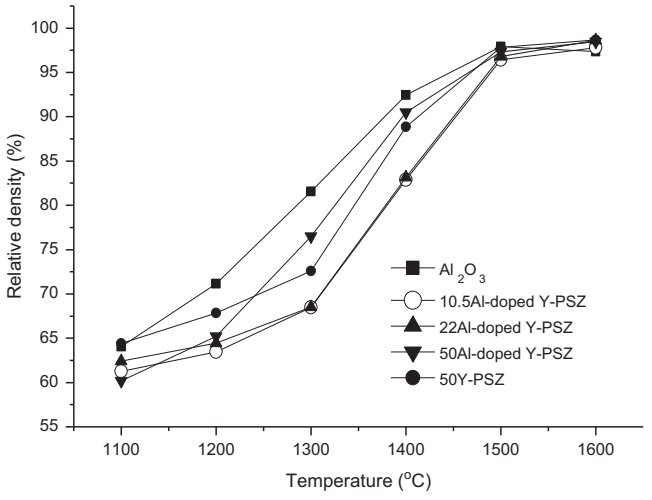

Fig. 3. Relative sintered density versus sintering temperature curves of Al_2O_3, 10.5Al-doped Y-PSZ, 22Al-doped Y-PSZ, 50Al-doped Y-PSZ and 50Y-PSZ.

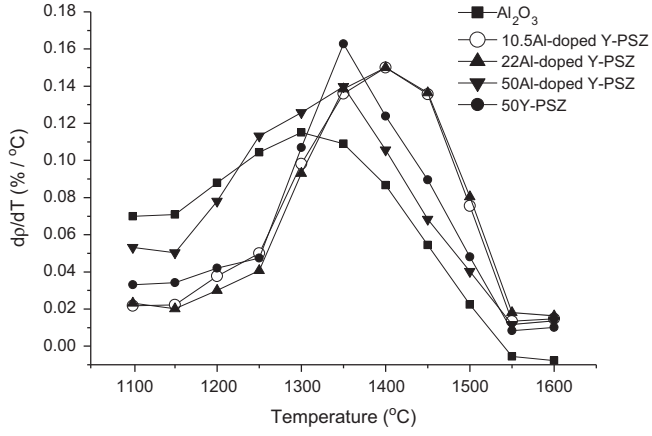

Fig. 4. Derivatives of sintered density with respect to temperature for Al_2O_3, 10.5Al-doped Y-PSZ, 22Al-doped Y-PSZ, 50Al-doped Y-PSZ and 50Y-PSZ.

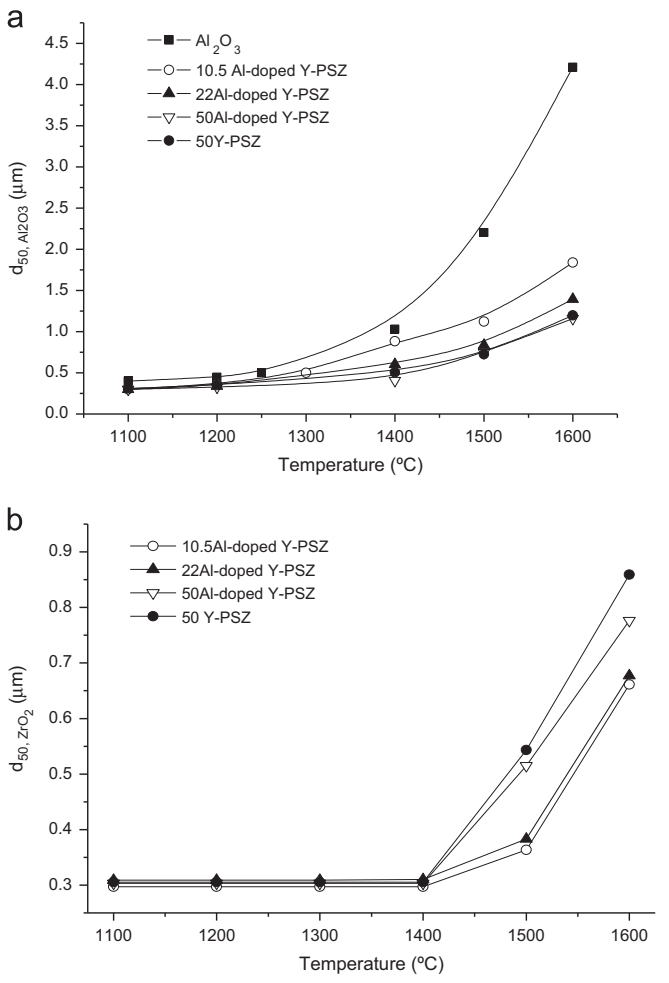

Fig. 5. Mean grain diameters (d_{50}) of (a) Al_2O_3 and (b) ZrO_2 as a function of the sintering temperature in the different composites.

On taking logarithms, the following equation is obtained:

$$\log\left(\frac{\Delta L}{L_0}\right) = n\log\left(\frac{K\gamma\Omega D}{kTa^p}\right) + \log(t) \quad (2)$$

Where $\Delta L=(L_0–L)$ is the change in length of the specimen, L_0 the initial length, K a numerical constant, γ the surface energy, Ω the atomic volume, D the diffusion coefficient, t the time, T the absolute temperature, k Boltzmann's constant, a the spherical particle radius, and the parameters n and p the order depending on the diffusion mechanism. The values of p for grain-boundary diffusion (GBD) and volume diffusion (VD) are $p=4$ and $p=3$, respectively. Eq. (1) is applicable to the fractional shrinkage of <4, which satisfy the intermediate sintering stage. Moriyoshi and Komatsu [12] have reported that the log $(\Delta L/L_0)$–log t plot of Eq. (2) does not show linear relationship when the grain growth proceeds simultaneously. Thus, the isothermal sintering experiments should be analyzed carefully since the log–log plot of the shrinkage curve depends not only on the diffusion coefficient but also on the grain size. Therefore, the mean grain diameters of Al_2O_3 and ZrO_2 in the different compacts were measured as a function of the sintering temperature and are shown in Fig. 5a and b, respectively.

The Al_2O_3 grain diameter in pure alumina remained nearly constant in the temperature range 1100–1250 °C, then a slightly increased in the grain diameter with increasing sintering temperature up to 1400 °C was found, followed by a significant increase with further increase in temperature up to 1600 °C. The Al_2O_3 grain diameter in the composites remained

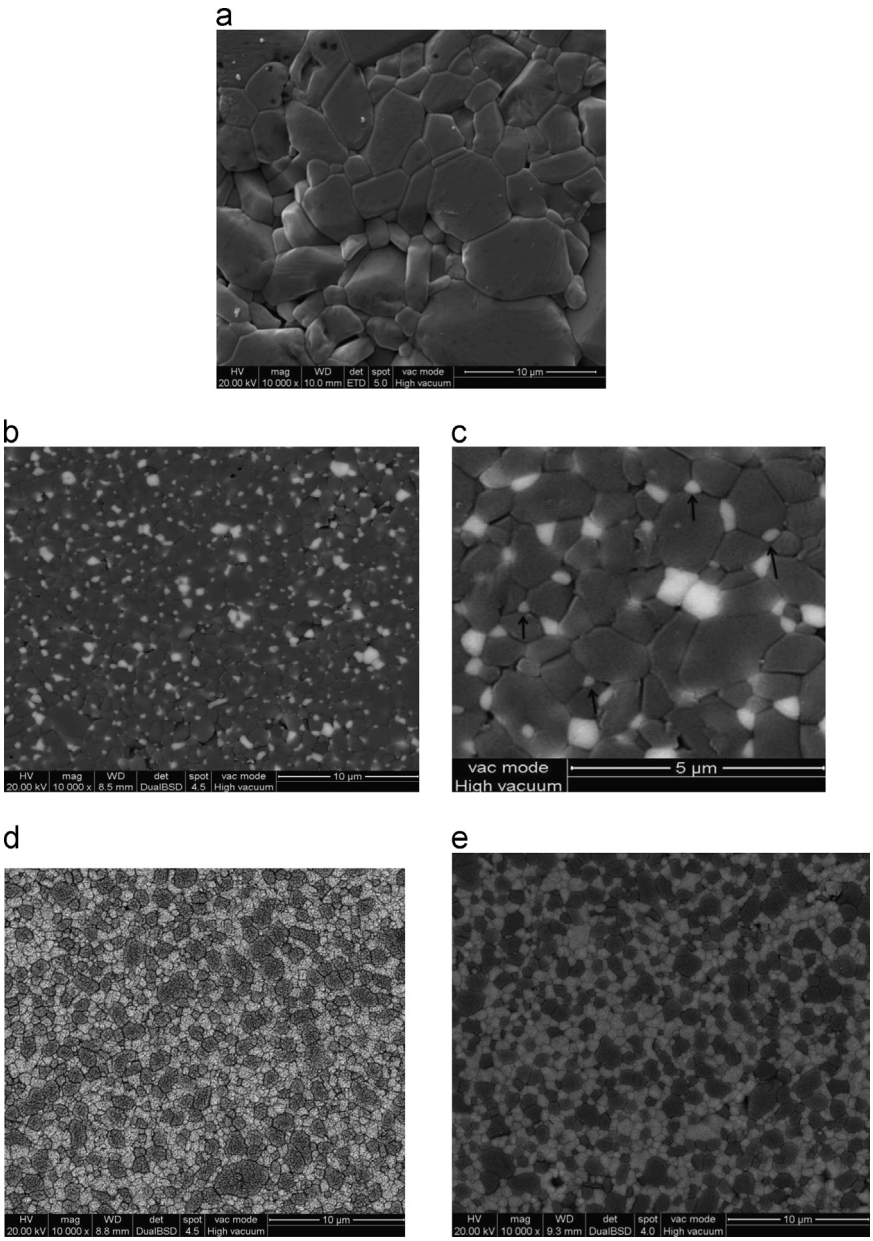

Fig. 6. SEM micrographs of different samples sintered at 1600 °C: (a) Al_2O_3; (b and c) 10.5Al-doped Y-PSZ at low magnification (b), and high magnification (c), the bright ZrO_2 grains indicated by arrows are at the triple points between the dark Al_2O_3 grains; (d) 50Al-doped Y-PSZ; and (e) 50Y-PSZ.

virtually unchanged up to 1300 °C and 1400 °C for the composites with 10.5 and 22-50Al-doped Y-PSZ, respectively; thereafter a gradual increase in the Al_2O_3 grain diameter up to 1600 °C was observed. No significant differences in the Al_2O_3 grain diameter versus temperature curve between 50Al-doped Y-PSZ and 50Y-PSZ was found.

Fig. 6 shows the microstructure of Al_2O_3, 10.5Al-doped Y-PSZ, 50Al-doped Y-PSZ and 50Y-PSZ sintered at 1600 °C. The micrographs (b–e) show ZrO_2 grains (the brighter phase) homogeneously distributed in a fine grain Al_2O_3 matrix (the darker phase). The ZrO_2 grains inhibited the Al_2O_3 grain growth during the final sintering stage (1400–1600 °C); thus, the ZrO_2 particles occupied the intergranular boundaries and often the triple points between Al_2O_3 grains (Fig. 6c). This had the effect of pinning the alumina and prevented grain growth. This pinning effect became larger as the ZrO_2 concentration in the composites increased; a greater number of ZrO_2 particles could pin the Al_2O_3 grain boundaries resulting in a lesser Al_2O_3 grain growth. 50 vol% ZrO_2 was the most effective concentration in inhibiting Al_2O_3 grain growth (Fig. 5a). As the Al-doped Y-PSZ content decreased from 50 to 10.5 vol% the Al_2O_3 grains began to grow at lower temperatures and the ZrO_2 efficiency in preventing Al_2O_3 grain growth was significantly reduced. For Al_2O_3 the rapid grain growth at 1400–1600 °C let to a grain diameter at 1600 °C that was 3.6 times greater than the grain diameter obtained for the composites with 50 vol% ZrO_2 (Fig. 5a).

Fig. 7 shows the Al_2O_3 grain diameter distribution curves for Al2O3, 10.5, 22 and 50Al-doped Y-PSZ at 1600 °C. Alumina showed an unimodal distribution with grain diameters between 0.5 and 12 μm, the more frequent grain diameter was 3 μm. The 10.5Al-doped Y-PSZ curve was significantly shifted to lower diameters with respect to that of Al_2O_3; the grain diameters were in the range 0.5–4 μm and the more frequent grain diameter of 1.5 μm was found. The Al_2O_3 grain diameter distribution became narrow and smaller with increasing the Al-doped Y-PSZ content from 10.5 to 50 vol%. For 22 and 50Al-doped Y-PSZ the more frequent grain diameters were 1.2 and 0.8 μm, respectively; almost all the Al_2O_3 grains could be kept below 2.7 μm for 50Al-doped Y-PSZ.

For all the composites, the ZrO_2 mean grain diameter remained nearly constant from 1100 to 1400 °C (Fig. 5b); a greater increase in the ZrO_2 grain diameter with increasing sintering temperature up to 1600 °C was found for the composites with 50 vol% ZrO_2. For 50Al-doped Y-PSZ the rapid zirconia grain growth occurred at $T > 1400$ °C, while for 10.5 and 22Al-doped Y-PSZ it appeared at $T > 1500$ °C. An increase in the Al-doped Y-PSZ concentration over 22 vol% increased the contacts between zirconia particles approaching each other and promoting their growth. However, the substitution of 50 vol% Al-doped Y-PSZ by Y-PSZ in the composites produced a slight increase in the ZrO_2 grain diameter at 1500–1600 °C. Thus, the ZrO_2 grain diameter versus T curves were opposite to those of Al_2O_3 grain diameter versus T curves (Fig. 5a and b), as the zirconia content increased the Al_2O_3 grain growth was lesser whereas the ZrO_2 grain growth became greater.

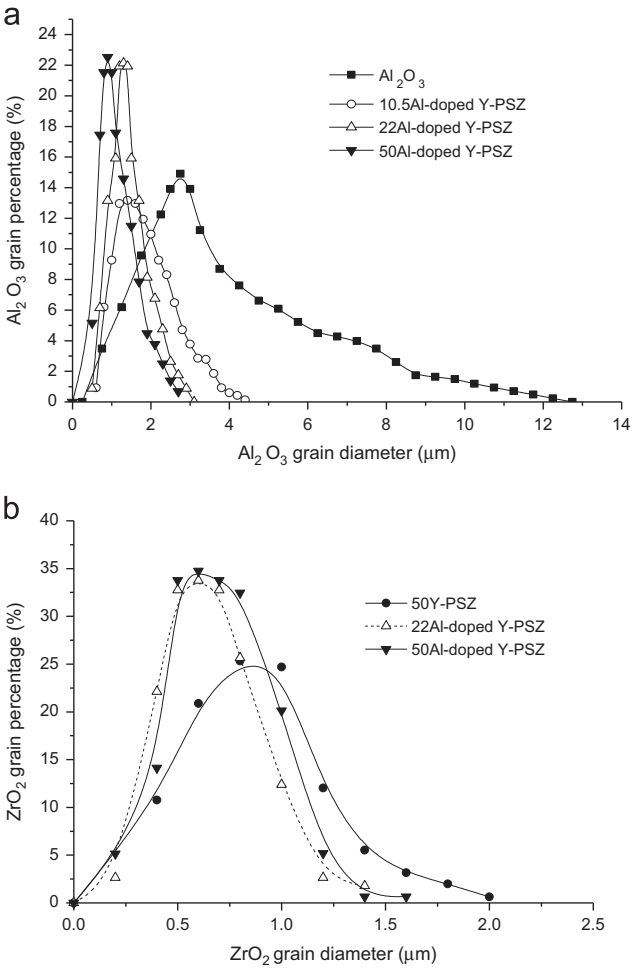

Fig. 7. (a) Al_2O_3 grain diameter distribution curves for Al_2O_3, 10.5Al-doped Y-PSZ, 22Al-doped Y-PSZ and 50Al-doped Y-PSZ at 1600 °C, (b) ZrO_2 grain diameter distribution curves for 22Al-doped Y-PSZ, 50Al-doped Y-PSZ and 50Y-PSZ at 1600 °C.

The ZrO_2 grain diameter distribution curves for 22Al-doped Y-PSZ, 50Al-doped Y-PSZ and 50Y-PSZ are shown in Fig. 7b. A greater volume of grains in the range 0.5–1.25 μm were found for 50Al-doped Y-PSZ with respect to 22 Al-doped Y-PSZ. The 50Al-doped Y-PSZ curve was slightly shifted to lower grain diameters with respect to that of 50Y-PSZ; thus a greater volume of finer diameters in the range 0.3–0.9 μm and a lesser volume of grains between 0.9 and 1.6 μm were observed. The most frequent grain diameter was 0.6 and 0.9 μm for 50Al-doped Y-PSZ and 50Y-PSZ, respectively. The smaller ZrO_2 grain diameter obtained at 1600 °C for 50Al-doped Y-PSZ with respect to 50Y-PSZ (Figs. 5b and 7b) was attributed to the finer 50Al-doped Y-PSZ particles relative to those of Y-PSZ (Fig. 1).

The above mentioned results could be summarized as follows: (1) the sintering temperature at which the Al_2O_3 grains did not change was 1150–1250 °C for Al_2O_3, 1150–1300 °C for 10.5Al-doped Y-PSZ, 1250–1400 °C for 22Al-doped Y-PSZ, 50Al-doped Y-PSZ and 50Y-PSZ. These temperature ranges were selected to analyze the isothermal shrinkage curves of each sample, (2) 50 vol% ZrO_2 was the most effective concentration to reduce the rate of Al_2O_3 grain

growth at the final sintering stage, (3) the Al_2O_3 grain growth began at lower temperatures and became greater with decreasing the Al-doped Y-PSZ content, (4) for pure Al_2O_3 the rapid grain growth at 1600 °C let to a grain diameter at 1600 °C which was 3.6 times greater than that obtained for 50Al-doped Y-PSZ, (5) as the Al-doped Y-PSZ content in the composites increased, the Al_2O_3 grain growth at the final sintering stage decreased while the ZrO_2 grain growth slightly increased,

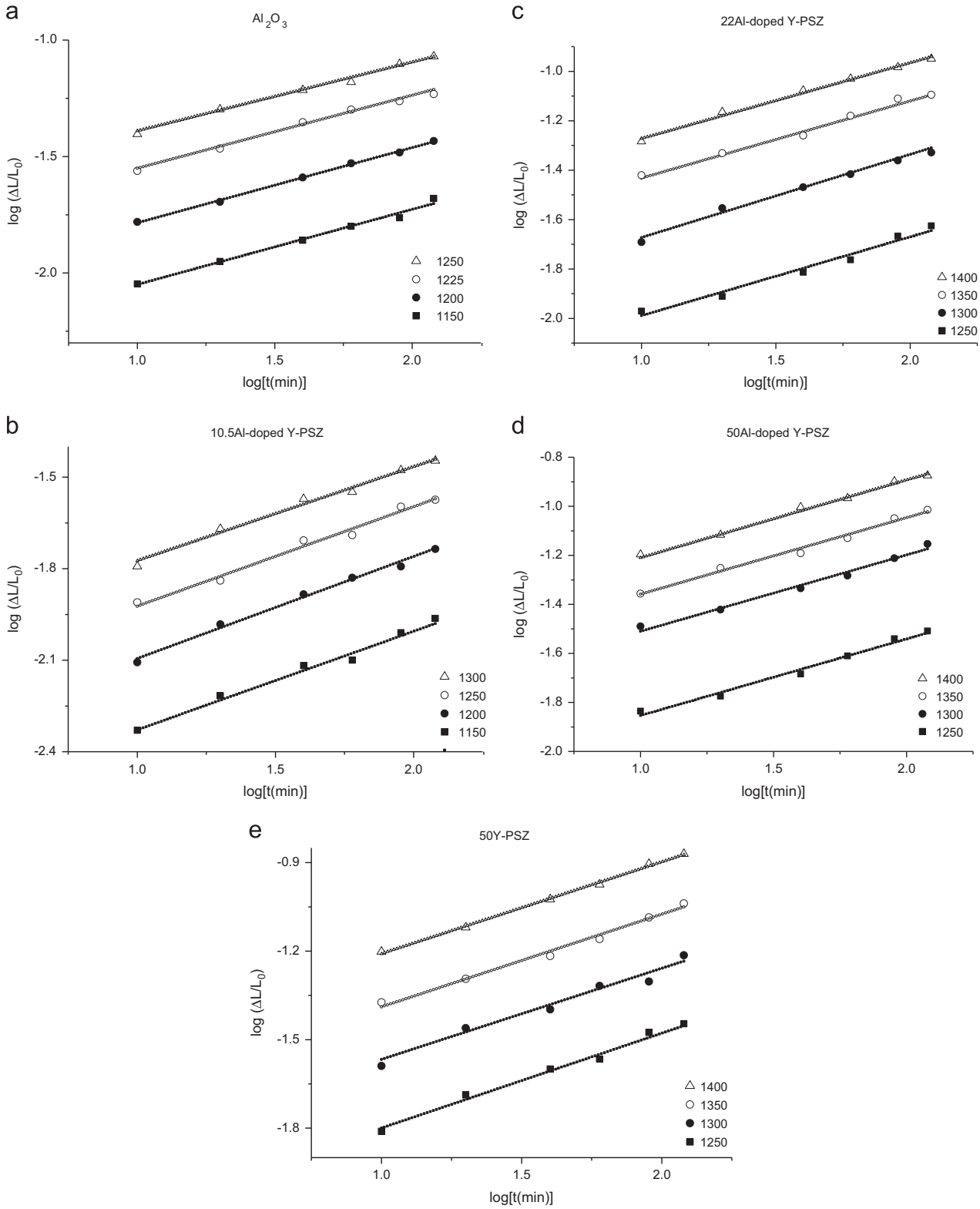

Fig. 8. Logarithm shrinkage–Logarithm time plots of: (a) Al_2O_3, (b) 10.5Al-doped Y-PSZ, (c) 22Al-doped Y-PSZ, (d) 50Al-doped Y-PSZ and (e) 50Y-PSZ at four different temperatures.

(6) the substitution of 50 vol% Y-PSZ by 50 vol% Al-doped Y-PSZ resulted in smaller ZrO_2 grains at 1600 °C.

3.3. Isothermal shrinkage analysis

Fig. 8 shows the log–log plots of the isothermal shrinkage versus heating time curves for Al_2O_3, 10.5Al-doped Y-PSZ, 22Al-doped Y-PSZ, 50Al-doped Y-PSZ and 50Y-PSZ at four different temperatures. All the log–log plots showed linear relationships and the data satisfactory fitted to a slope of 1/3 ($n=1/3$, Eq. (2)). These results indicated that the sintering rate of Al_2O_3 and the composites was controlled by grain boundary diffusion mechanism (GBD).The activation energy and frequency factor term of each specimen were estimated using the values of the constant term in Eq. (2). This constant term corresponded to the intercept of the straight line on the vertical axis in Fig. 8 when log t is 0. Using as $\beta=(K\gamma\Omega D)/(kTa^p)$ (Eq. (2)) and using the general expression of the diffusion coefficient, $D=D_0\exp(-Q/RT)$ the following equation is obtained:

$$\beta T=\beta_0\exp\left(\frac{-Q}{RT}\right) \tag{3}$$

where

$$\beta_0=\frac{K\gamma\Omega D_0}{ka^p} \tag{4}$$

On taking natural logarithm in Eq. (3) resulted in

$$\ln(\beta T)=\ln\beta_0-\frac{Q}{RT} \tag{5}$$

where Q is the activation energy, R the gas constant, and D_0 the preexponential term of the diffusion coefficient.

Fig. 9 shows the Arrhenius-type plots of $\ln(\beta T)$ against $1/T$ for Al_2O_3 and the different composites. The plots of all specimens showed linear relationships; the Q value of each sample was determined from the slope of the straight line by applying Eq. (5) to the Arrhenius-type plot in Fig. 9. The value of β_0 was also determined from the intercept of the straight line on the vertical axis when $1/T=0$. The Q and β_0 values of Al_2O_3 and the different composites are presented in Table 2. The activation energy of GBD in Al_2O_3 was smaller than that of the Al_2O_3–ZrO_2 composites, the behavior of β_0 also revealed tendencies similar to that of Q (Table 2). Thus, the greater sintering rate of Al_2O_3 with respect to that of the composites was attributed to the lower activation energy value (Eqs. (1)–(5)).

At intermediate-stage sintering of alumina, Young et al. [13] and Wang et al. [7] measured an activation energy of 480 ± 42 and 440 ± 40 KJ/mol, respectively. In the case of alumina–zirconia, our measurements of the activation energy agreed well with the work of Wakai et al. [14] who obtained the following values for alumina–zirconia (3 mol% yttria): 723 KJ/mol for 50 vol% Al_2O_3 and 681 KJ/mol for 85.7 vol% Al_2O_3. Wang et al. [15] also reported an activation energy of 730 ± 60 KJ/mol for alumina containing 5 vol% ZrO_2; they correlated the activation energies of alumina and alumina/zirconia with their respective interfacial energies. The alumina/zirconia interface energy was lower than that of alumina/alumina by a factor of 1.5 which was nearly the same as the ratio of the activation energies for boundary diffusion in these two types of interfaces [15]. Our results also showed that the activation energy remained nearly constant with increasing the Al-doped Y-PSZ content from 10.5 to 50 vol% (Table 2); besides, the activation energy values of the composites with 50 vol% of Y-PSZ and Al-doped Y-PSZ were similar. However, the densification rate at the intermediate stage of 50Al-doped Y-PSZ was enhanced compared with the others composites (Fig. 3).

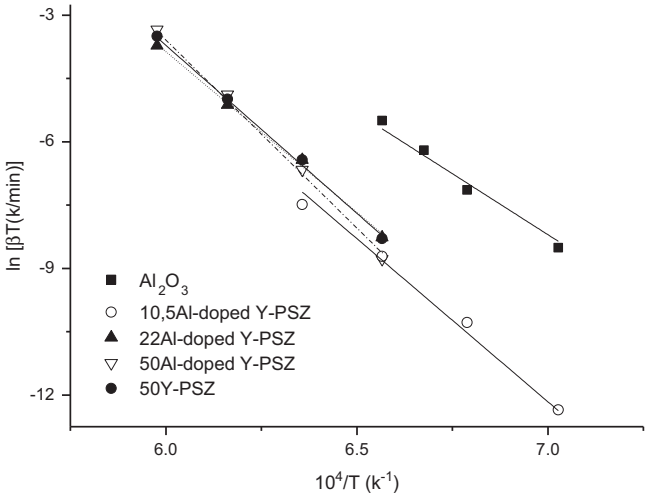

Fig. 9. Arrhenius-type plots of $\ln(\beta T)$ against $1/T$ for Al_2O_3 and the different composites.

Using β, Eq. (1) is expressed by the following equation:

$$\frac{\Delta L}{L_0}=\beta^n t^n \tag{6}$$

Substituting Eq. (3) into Eq. (6) gives:

$$\frac{\Delta L}{L_0}=\left[\left(\frac{{\beta_0}^n}{T^n}\right)\exp\left(\frac{-nQ}{RT}\right)\right]t^n \tag{7}$$

Under the same diffusion mechanism (namely, a constant n), the sintering rate could be compared in the magnitude of β, and increased with increasing β. The increase in β_0 under a constant Q and T let to an increase in β and consequently in the sintering rate (Eqs. (6) and (7)). The results presented in Table 2 revealed that there was a little change in the Q values of grain-boundary diffusion within the composites but β_0 increased with an increase in the Al-doped Y-PSZ content from 22 to 50 vol%, the substitution of 50 vol% Y-PSZ by Al-doped Y-PSZ also increased the β_0 value. Matsui et al. [11] studied the effect of the specific surface area of different zirconia powders on the initial sintering stage; they concluded that the increase in the specific surface area of fine zirconia powders enhanced the shrinkage rate because of an increase in β_0. In the present work, the specific surface area of the Al-doped Y-PSZ particles was markedly higher than that of Al_2O_3 or Y-PSZ (Section 3.1), consequently a higher β_0 value could be expected when a large amount of Al_2O_3 or Y-PSZ was substituted by Al-doped Y-PSZ. Therefore, the increase in

Table 2
Activation energies and frequency factors of diffusion at the intermediate stage of sintering for Al_2O_3 and the different composites.

Specimen	Activation energy (KJ/mol)	Frequency factor ln[β_0 (s^{-1})]
Al_2O_3	480 ± 20	32
10.5Al-doped Y-PSZ	644 ± 20	40
22Al-doped Y-PSZ	660 ± 10	41
50Al-doped Y-PSZ	690 ± 20	51
50Y-PSZ	670 ± 20	43

the β_0 value with increasing Al-doped Y-PSZ content from 22 to 50 vol% or with the substitution of 50 vol% Y-PSZ by Al-doped Y-PSZ was a consequence to the increase in the specific surface area of the powders, resulting in an increasing sintering rate.

Matsui et al. [16] also investigated the effect of Al_2O_3 concentration on the sintering of fine ZrO_2 powders; they demonstrated that an increase in the Al_2O_3 content from 0 to 1 wt% enhanced the densification rate because of the increase in both n with the change of diffusion mechanism from grain boundary to volume diffusion and β_0 (Eq. 7). This enhanced sintering mechanism was reasonably interpreted by the segregated dissolution of Al_2O_3 at ZrO_2 grain boundaries [16]. Therefore, the higher sintering rate at the intermediate stage of 50Al-doped Y-PSZ relative to 10.5-22Al-doped Y-PSZ and 50 Y-PSZ could be attributed to the increase in the specific surface area of the powders together with the enhanced densification produced by the Al_2O_3 doping.

3.4. Sample hardness

Fig. 10 shows the vickers hardness (H_v) versus the sintering temperature for Al_2O_3 and the different composites. For all the samples the hardness increased with increasing sintering temperature from 1300 to 1400 °C as a consequence of the increase in the relative sintered density (Fig. 3). Thus, at 1300–1400 °C the higher relative sintered density of Al_2O_3 resulted in higher H_v values; for the composites the hardness increased with increasing the Al-doped Y-PSZ content from 22 to 50 vol% in accordance with the sintered density results. Although the sintered density of Al_2O_3 increased with further increasing in temperature from 1400 to 1500 °C, a maximum hardness was found at 1400 °C; this H_v maximum was shifted to 1500 °C for 10.5Al-doped Y-PSZ. On the contrary, the H_v vs. T curves for 22–50 Al-doped Y-PSZ and 50 Y-PSZ did not show a maximum instead the H_v value increased up to 1600 °C. This behavior was related with the Al_2O_3 grain growth versus temperature curves shown in Fig. 5a. When the Al_2O_3 average grain diameter increased over about 1 μm a markedly decrease in the H_v values was found; this occurred at $T > 1400$ and 1500 °C for Al_2O_3 and 10.5Al-doped Y-PSZ, respectively. According to Rice et al. [17] the generally accepted trend was that H_v increased with decreasing the grain size (G) (e.g., $H_v \propto G^{-1/2}$) at finer G. For their alumina specimens, Krell et al. [18] attributed the increase in hardness with decreasing grain size to a reduction in dislocation mobility with decreasing grain size.

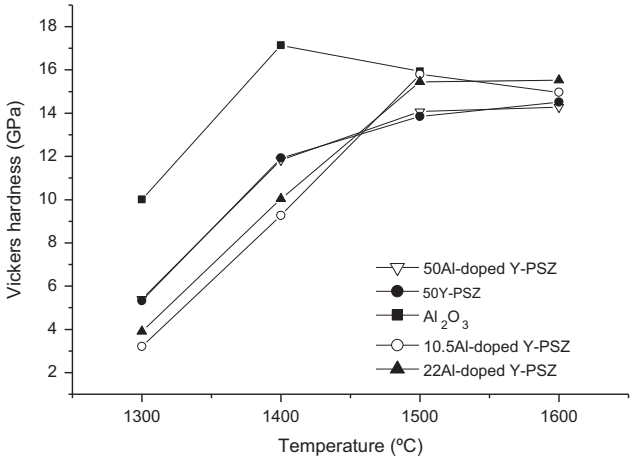

Fig. 10. Vickers hardness versus the sintering temperature for Al_2O_3 and the different composites.

In this work, we reported a decrease in the H_v values when the Al_2O_3 became greater than about 1 μm, this occurred at $T > 1400$ °C for Al_2O_3 and $T > 1500$ °C for 10.5Al-doped Y-PSZ. Since 22 and 50 vol% ZrO_2 reduced the rate of Al_2O_3 grain growth (Fig. 5a), the Al_2O_3 average grain diameter remained ≤ 1 μm up to 1600 °C and consequently a decrease in H_v was not observed (Fig. 10). 50Al-doped Y-PSZ and 50Y-PSZ exhibited nearly the same H_v–T dependence in the whole range of temperatures studied. The H_v value for Al_2O_3 at 1400 °C was markedly higher than that of 50 Al-doped Y-PSZ and 50Y-PSZ at 1600 °C; since alumina is harder than ZrO_2 [6], these differences in the H_v values could be attributed to the greater substitution of Al_2O_3 by ZrO_2 in the composites. The lowest H_v values in the temperature range 1500–1600 °C were found for the composites with 50 vol% ZrO_2, this should lead a priori to lower wear resistance.

4. Conclusions

Two commercial 3 mol% yttria-partially stabilized zirconia powders, 0.3 wt% Al_2O_3-doped (Al-doped Y-PSZ) and without Al_2O_3 (Y-PSZ), were used to produce alumina (Al_2O_3)–zirconia (ZrO_2) slip cast composites. The influence of the substitution of Al_2O_3 either by different Al-doped Y-PSZ contents or 50 vol% Y-PSZ on the sintering kinetic at the intermediate stage was investigated. In addition, the microstructure of Al_2O_3 and the different composites at temperatures in the range of 1100–1600 °C was studied and related to the sample hardness.

The intermediate sintering stage of both alumina and the composites was controlled by a grain-boundary diffusion mechanism. The densification rate of Al_2O_3–ZrO_2 was lower than that of Al_2O_3 as a consequence of the increase in the activation energy of sintering in the presence of zirconia. An increase in the sintering rate was observed when Al-doped Y-PSZ increased from 22 to 50 vol% or when 50 vol% Y-PSZ was substituted by 50 vol% Al-doped Y-PSZ. This behavior could be attributed to the increase in the specific surface area of the Al-doped Y-PSZ powder together with the enhanced densification produced by the Al_2O_3 doping.

50 vol% ZrO_2 was the most effective concentration to reduce the rate of Al_2O_3 grain growth in the final sintering stage; the Al_2O_3 grain growth began at lower temperatures and became greater with decreasing the Al-doped Y-PSZ content. On the contrary, the ZrO_2 grain growth slightly increased with increasing the Al-doped Y-PSZ concentration from 22 to 50 vol%. However, for 50 vol% Al-doped Y-PSZ a smaller ZrO_2 grain size distribution compared with 50 vol% Y-PSZ could be achieved.

As the average Al_2O_3 grain size of the sintered samples became greater than about 1 μm a marked decrease in the hardness was found; this occurred at temperatures higher than 1400 °C and 1500 °C for Al_2O_3 and the composite with 10.5 vol% Al-doped Y-PSZ, respectively. Since 22 vol% Al-doped Y-PSZ, 50 vol% Al-doped Y-PSZ and 50 vol% Y-PSZ reduced the rate of Al_2O_3 grain growth a decrease in hardness up to 1600 °C was not observed.

References

[1] J. Wang, R. Stevens, Review zirconia-toughened alumina (ZTA) ceramics, J. Mater. Sci. 24 (10) (1989) 3421–3440.

[2] S. Olhero, I. Ganesh, P. Torres, F. Alves, J.M.F. Ferreira, Aqueous colloidal processing of ZTA composites, J. Am. Ceram. Soc. 92 (1) (2009) 9–16.

[3] C. Piconi, G. Maccauro, Zirconia as a biomaterial, Biomaterials 20 (1999) 1–25.

[4] Y. Shin, Y. Rhee, S. Kang, Experimental evaluation of toughening mechanism in alumina–zirconia composites, J. Am. Ceram. Soc. 82 (5) (1999) 1229–1232.

[5] H.J. Hannink, P.M Kelly, B.C. Muddle, Transformation toughening in zirconia-containing ceramics, J. Am. Ceram. Soc. 83 (3) (2000) 461–487.

[6] A.H. De Aza, J Chevalier, G. Fantozzi, M. Schehl, R. Torrecillas, Crack growth resistance of alumina, zirconia and zirconia toughened alumina ceramics for joint prostheses, Biomaterials 23 (2002) 937–945.

[7] J. Wang, R. Raj, Estimate of the activation energies for boundary diffusion from rate-controlled sintering of pure alumina, and alumina doped with zirconia or titania, J. Am. Ceram. Soc. 73 (5) (1990) 1172–1175.

[8] K. Matsui, N. Ohmichi, M. Ohgai, N. Enomoto, J. Hojo, Sintering kinetics at constant rates of heating: effect of Al_2O_3 on the initial sintering stage of fine zirconia powder, J. Am. Ceram. Soc. 88 (12) (2005) 3346–3352.

[9] F.F. Lange, D.J. Green, Effect of inclusion size on the retention of tetragonal ZrO_2: theory and experiments, Advances in Ceramics, Science and Technology of Zirconia, vol. 3, , 1981, p. 222–223.

[10] H.L. Calambás Pulgarin, L.B. Garrido, M.P. Albano, Processing of different alumina-zirconia composites by slip casting, Ceram. Int. 39 (6) (2013) 6657–6667.

[11] K. Matsui, A. Matsumoto, M. Uehara, N. Enomoto, J. Hojo, Sintering kinetics at isothermal shrinkage. Effect of specific surface area on the initial sintering stage of fine zirconia powder, J. Am. Ceram. Soc. 90 (1) (2007) 44–49.

[12] Y. Moriyoshi, W. Komatsu, Kinetics of initial sintering with grain growth, J. Am. Ceram. Soc. 53 (12) (1970) 671–675.

[13] W.S. Young, I.B. Cutler, Initial sintering with constant rates of heating, J. Am. Ceram. Soc. 53 (12) (1970) 659–663.

[14] F. Wakai, Y. Kodama, S. Sakorguchi, M. Murayama, H. Kato, T. Nagone, Proceedings of the MRS International Meeting on Superplasticity, Materials Research Society, Pittsburgh, PA, 1989, p. 259.

[15] J. Wang, R. Raj, Activation energy for the sintering of two-phase alumina/zirconia ceramics, J. Am. Ceram. Soc. 74 (8) (1991) 1959–1963.

[16] K. Matsui, T. Yamakawa, M. Uehara, N. Enomoto, J. Hojo, Mechanism of alumina-enhanced sintering of fine zirconia powder: influence of alumina concentration on the initial stage sintering, J. Am. Ceram. Soc. 91 (6) (2008) 1888–1897.

[17] R.W. Rice, C.C. Wu, F. Borchelt, Hardness-grain-size relations in ceramics, J. Am. Ceram. Soc. 77 (10) (1994) 2539–2553.

[18] A. Krell, P. Blank, Grain size dependence of hardness in dense submicrometer alumina, J. Am. Ceram. Soc 78 (4) (1995) 1118–1120.